MINISTRY OF EDUCATION AND TRAINING

VIETNAM ACADEMY OF SCIENCE AND TECHNOLOGY

GRADUATE UNIVERSITY OF SCIENCE AND TECHNOLOGY

Nguyen Dien Trung

SYNTHESIZING TITANATE-BASED CATALYST FOR CINNAMIC ACID PHOTODEGRADATION IN WATER

Major: Theoretical chemistry and physical chemistry

Code: 9440119

SUMMARY OF THEORETICAL CHEMISTRY AND PHYSICAL CHEMISTRY DOCTORAL THESIS

HO CHI MINH – 2023

The doctoral thesis was completed at the Academy of Science and Technology - Vietnam Academy of Science and Technology

Supervisor 1: Dr. Hoang Tien Cuong

Supervisor 2: Dr. Ha Cam Anh

Reviewer 1: ……

Reviewer 2: ……

Reviewer 3: ……

This doctoral thesis will be defended at the Board of Examiners of Graduate University of Science and Technology, Vietnam Academy of Science and Technology on hour …., date …. month ….. 2023

This doctoral thesis can be explored at:

- Library of the Graduate University of Science and Technology
- National Library of Vietnam

INTRODUCTION

1. The urgency of the thesis

Nowadays, water pollution is a concerning issue in modern society and affects the balance of the ecosystem. Water sources are polluted by toxic organic substances generated from agricultural and industrial activities. Among those pollutants, phenolic acid compounds are becoming more and more worrisome. Phenolic acid compounds are difficult to degrade and harmful to microorganisms in water, just at a low concentration. Therefore, the purification of water sources and the removal of phenolic acid compounds have become a pressing problem in recent years. Various treatment methods have been proposed, including adsorption and desorption, incineration, and biodegradation. However, the proposed methods have been ineffective, high-cost, difficult operating conditions, and incomplete treatment. Among them, the photocatalytic degradation of phenolic acid using photocatalysts is considered an effective solution. The highlights of photocatalysts in the degradation of phenolic acids are low cost, high efficiency, good stability, and non-toxicity. In addition, the reaction is carried out at room temperature and atmospheric pressure, forming friendly products such as CO_2, H_2O**,** and inorganic acids. In addition to a traditional photocatalyst TiO_2 recognized as a highly efficient UV-photocatalyst, titanate-based perovskites and titanate-based pseudobrookites also attract much attention in study. These titanate-based catalysts have good visible light absorption thanks to their low band gap. Additionally, combining metal oxide with TiO_2 enhances light absorption, improves the specific surface area, and limits electron-hole recombination, which is considered a promising photocatalyst.

2. The objectives of the thesis

The doctoral thesis "Synthesizing titanate-based catalyst for cinnamic acid photodegradation in water" achieves the following objectives: (i) successfully synthesizing three photocatalytic groups: TiO_2; titanate-perovskites and titanate-pseudobrookites; titanate-perovskite/TiO_2 and titanate-pseudobrookites/TiO_2 having good activity for photodegradation of cinnamic acid (CA); (ii) elucidating the relationship between the composition, physicochemical properties and photolytic activities of the

catalysts; and (iii) investigating and proposing the kinetics of the CA degradation process on typical catalysts.

In the present study, TiO_2 catalyst was synthesized by the hydrothermal method in different media, titanate-perovskites and titanate-pseudobrookites was produced by sol-gel process and titanate-perovskite/TiO_2 and titanate-pseudobrookites/TiO_2 was created by hydrothermal combined sol-gel technique. The catalytic activity was evaluated for the photodegradation of cinnamic acid. From the obtained results, determine the suitable conditions for the synthesizing and photodegradation of cinnamic acid, elucidate the relationship between the characteristics and photoactivity of the prepared catalysts; and propose the kinetics of cinnamic acid degradation on the catalysts with high conversion.

3. The main contents of the thesis

To achieve the set objectives, the thesis "Synthesizing titanate-based catalyst for cinnamic acid photodegradation in water" implements the following contents: (i) synthesizing three groups of catalysts (TiO_2; titanate-perovskites and titanate-pseudobrookites; titanate-perovskite/TiO_2 and titanate-pseudobrookites/TiO_2), (ii) investigating the photoactivity of three catalyst groups (TiO_2; titanate-perovskites and titanate-pseudobrookites; titanate-perovskite/TiO_2 and titanate-pseudobrookites/TiO_2) for the CA photodegradation, (iii) surveying the physicochemical properties of the synthesized catalysts, (iv) investigating and proposing the kinetics of the CA degradation process on typical catalysts. The obtained results determined the relationship between the composition, the method of catalytic synthesis, the physicochemical properties, the photocatalytic activity, and the kinetic characteristics of the CA photodegradation.

4. Novelty of the thesis

It has been confirmed that changing the hydrothermal medium is possible to control the main physicochemical and photochemical properties, such as phase composition, bandgap energy, and zero charge points. In addition, the TiO_2 catalyst hydrolyzed in an acidic medium shows better photocatalytic activity than commercial TiO_2 P25, while the TiO_2 catalyst hydrolyzed in an aqueous medium is more environmentally friendly in manufacturing and easier to recover than P25.

Titanate-perovskites ($CoTiO_3$) and titanate-pseudobrookites (Al_2TiO_5, Fe_2TiO_5) were successfully synthesized by the sol-gel method at low calcination temperature. Especially, Al_2TiO_5 pseudobrookite is recognized as a novel photocatalyst with high photoactivity, long-term stability, and easy recovery.

The heterostructure catalysts: Al_2TiO_5/TiO_2, Fe_2TiO_5/TiO_2, and $CoTiO_3/TiO_2$ were successfully synthesized by sol-gel-based hydrothermal method using an environmentally friendly solvent. The synthesized materials present larger specific surface areas, outstanding photocatalytic activity, more long-term stability, and easier recovery than TiO_2 catalysts.

The kinetics of the photooxidation of cinnamic acid under UV-A light irradiation is comprehensively studied. The kinetic equation is proposed based on the summing of research results on the influence of factors such as the reactants, presence of intermediates, light intensity, especially, quantification of the role of oxidizing agents (holes h^+, hydroxyl radicals $HO^\bullet$ and superoxide radicals $OO^{\bullet-}$).

5. Thesis structure

The content of the doctoral thesis is presented in 116 pages (excluding the appendix 125 pages). The thesis is divided into three chapters: Chapter 1. Overview (29 pages), Chapter 2. Experimental methods (10 pages), Chapter 3. Results and discussion (77 pages), and Conclusions and recommendations (2 pages). The thesis contained 22 Tables, 69 Figures, and 258 references.

CHAPTER 1. OVERVIEW

Chapter 1 presents an overview of (i) the situation of water pollution, (ii) the properties and toxicity of phenolic acids, (iii) the photoreaction mechanism, the role of oxidizing agents, and the influencing factors on the photocatalytic activity, (iv) advantages and disadvantages of the photocatalytic groups: TiO_2; perovskites and pseudobrookites; perovskite/TiO_2 and pseudobrookites/TiO_2, (v) synthesis methods for photocatalytic materials, (vi) kinetics of the photodegradation of organic compounds in water processes.

In the near future, the scarcity of clean water will be the leading threat to global humanity. According to a recent report by the World Health

Organization, approximately 50% of people will maintain their lives in areas of water scarcity by 2025, while the clean water demand in the industry will reach the top. Although water is the most abundant natural resource on Earth, only about 1% of the water is available to humans. Clean water prices are increasing with climate change and population growth. The prominent problem people face now is seriously polluted water sources by toxic organic and inorganic substances unsuitable for domestic use and production activities. In nature, phenolic acids account for about one-third of phenolic compounds. Phenolic acids are classified into two main kinds: hydroxybenzoic acid and hydroxycinnamic acid. Generally, hydroxycinnamic acid is more common than hydroxybenzoic acid and is present in free or conjugated forms. Free hydroxycinnamic are products of the chemical or enzymatic hydrolysis during extraction. Common compounds are esters of hydroxycinnamic acid.

Titanate-based perovskites and titanate-based pseudobrookites benefit from photodegradation due to their low bandgap energy and intensive absorption of visible light. However, these catalysts have low photoactivity because of low specific surface area and electron mobility. A logical strategy combines low bandgap titanate-based catalysts with high electron mobility TiO_2 to form a heterostructure system with a large specific surface area and good electron-hole separation. Among the chemical methods for synthesizing photocatalysts, the most popular are sol-gel and hydrothermal methods.

The efficiency of the photocatalytic reaction is influenced by not only the catalyst but also the reaction conditions, such as catalyst dosage, dissolved O_2 concentration, solution pH, and light intensity. The investigation of the kinetics of photodegradation reaction in the liquid phase has been limited. In most of the published photocatalytic reactions in the liquid phase, the Langmuir-Hinshelwood mechanism is accepted.

CHAPTER 2. EXPERIMENTAL METHODS

Chapter 2 presents (i) method for synthesizing three photocatalysts: TiO_2; titanate-perovskites and titanate-pseudobrookites; titanate-perovskite/TiO_2 and titanate-pseudobrookites/TiO_2, (ii) methods for characterizing the properties and surveying photocatalytic activity of the

catalysts, (iii) methods for analyze intermediate compounds and oxidizing species, and (iv) methods for studying reaction kinetics.

2.1. Synthesis of catalysts

2.1.1. Synthesis of TiO_2 catalyst

TiO_2 catalyst was synthesized by hydrothermal method using precursor $(C_3H_7O)_4Ti$ (TTIP) in various media: 0.9 M HCl (Ti-a), water (Ti-w), and 1.0 M NaOH (Ti- b) at 160 °C-12 h. The influence of medium concentration, TTIP volume, temperature, and hydrothermal time was investigated to determine the most favorable condition. After being washed with C_2H_5OH and H_2O, the solid was dried at 60 °C-12 h to obtain a TiO_2 catalyst.

2.1.2. Synthesis of titanate-based perovskite and titanate-based pseudobrookite catalyst (MTO)

MTO catalyst, including Al_2TiO_5 (ATO), Fe_2TiO_5 (FTO), and $CoTiO_3$ (CTO), was synthesized by the sol-gel method using precursors: $Al(NO_3)_3.9H_2O$, $Fe(NO_3)_3.9H_2O$, and $Co(NO_3)_2.6H_2O$. Dissolve x_3 g of citric acid in x_1 mL of C_2H_5OH. Then, add x_2 g of $M(NO_3)_n.mH_2O$ to the obtained solution and stir it for 60 min to form a homogeneous solution. Next, add TTIP drop by drop to the solution until the end of 3.0 mL and continue to stir the mixture for 60 min to obtain a gel. A solid was obtained by drying this gel at 60 °C-12 h. Finally, the dried solid was calcined at T °C for t h to form the MTO catalyst.

2.1.3. Synthesis of titanate-perovskite/TiO_2 and titanate-pseudobrookite/TiO_2 catalyst (MTO/Ti)

3.0 mL TTIP was dropped into 40.0 mL water. Next, m g of MTO was added and the obtained solution was stirred for 30 min to obtain a mixture. The mixture was hydrolyzed at 160 °C-12 h. Centrifuge the mixture, filter the solids, and wash them with C_2H_5OH and H_2O. The xMTO/Ti catalysts (where x is the MTO content) were obtained by drying the solid at 60 °C-12 h.

2.2. Analysis of physicochemical properties

Various techniques were used to analyze the physicochemical properties of the catalysts. The phase composition was identified by X-ray

diffraction (XRD) and Raman scattering (Raman). Thermogravimetric analysis (TGA) was used to recognize the phase transition. The presence of OH groups on the catalyst surface was found in Fourier-transform infrared spectroscopy (FTIR). The specific surface area of samples was calculated according to the Brunauer-Emmett-Teller (BET) nitrogen adsorption isotherms. Diffuse reflectance spectroscopy (DRS) was used to determine the catalysts' diffuse reflectance and bandgap energy. The salt addition method determined the catalysts' points of zero charge (PZC). The elemental analysis of the synthesized samples was performed using dispersive energy X-ray (EDX). Scanning electron microscopy (SEM) and transmission electron microscopy (TEM) apparatuses were used to investigate the morphology and surface properties of the obtained materials.

2.3. Investigation of photocatalytic activity

The photocatalytic activity of CA degradation was studied by the batch method under the UV-A light with λ = 350–400 nm as a removing model for phenolic acid (Figure 2.1). The influence of the operation parameters, including the catalyst dosage, the initial pH solution, and the airflow rate, was investigated.

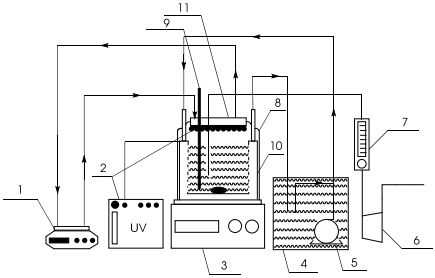

Figure 2.1. Schematic diagram of the photooxidation reactor system.

(1) pump, (2) control system of light, (3) magnetic stirrer, (4) water bath, (5) circulating pump, (6) oxygen blower, (7) flowmeter, (8) and (9) thermometer, (10) reaction vessel, (11) cooling system of UV-A lamp

2.4. Study of reaction kinetics

The reaction kinetics was carried out on six typical catalysts. The factors affecting the reaction rate, such as CA concentration, dissolved O_2 concentration, light intensity, h^+ concentration, $HO^\bullet$ concentration, and $OO^{\bullet-}$ concentration, were evaluated. The kinetic coefficients and orders of kinetic equations were determined by the least squares method with the solver tool in Microsoft Excel.

2.5. Analysis of the reaction mixture

Solution samples were analyzed on UV-Vis equipment after catalyst

filtration using a 0.22 μm pore-size polytetrafluoroethylene filter. In addition, the presence of intermediates was identified and quantified by HNMR.

CHAPTER 3. RESULTS AND DISCUSSION

3.1. TiO_2 catalyst

3.1.1. Effect of synthetic medium

Based on the investigation results of the influence of medium concentration, TTIP volume, temperature, and hydrothermal time the suitable conditions for the TiO_2 formation were determined as follows: using 40.0 mL of 0.9 M HCl solution (Ti-a sample), H_2O (Ti-w), and 0.1 M NaOH solution (Ti-b), 3.0 mL TTIP and hydrolyzed at 160 ^oC-12 h. The physico-chemical properties of the TiO_2 catalysts are summarized in Figure 3.1 and Table 3.1.

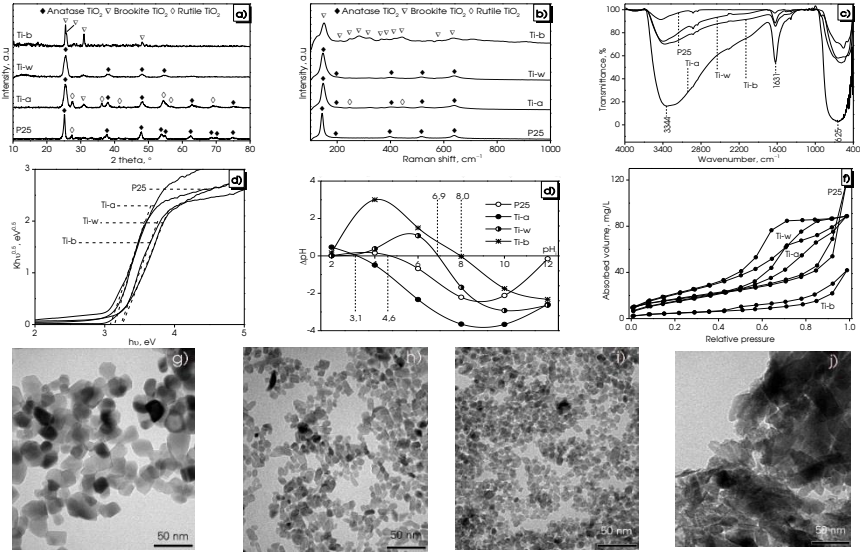

Figure 3.1. XRD pattern (a), Raman spectra (b), FTIR spectra (c), Tauc plot (d), the point of zero charges (e), adsorption-desorption isotherms (f), and TEM images: P25 (g), Ti-a (h), Ti-w (i), and Ti-b (j) of TiO_2 catalysts.

From the XRD pattern (Figure 3.1a) and Raman spectra (Figure 3.1b) of the TiO_2 catalysts, it can be seen that the hydrothermal medium significantly affects the phase of the synthesis of TiO_2. Ti-b sample containing the brookite phase was synthesized in the alkaline media;

meanwhile, the anatase phase was present in the composition of the Ti-w catalyst. The neutral solvent is favorable for the anatase phase. Meanwhile, the alkaline media is beneficial for forming the brookite phase. In contrast, the mixed phase (61.3% anatase, 18.0% rutile, 20.7% brookite) was formed on the Ti-a catalyst. Commercial Degusa P25 TiO_2 catalyst has a phase composition of 86.4% anatase and 13.6% rutile. The phase composition of the catalysts was also confirmed through Raman spectroscopy (Figure 3.1b).

FTIR spectra of the TiO_2 catalysts are illustrated in Figure 3.1c. The characteristic peaks assigned to the valence vibration of the OH group on the catalyst surface were observed on the FTIR spectra of all samples. Compared to the P25, Ti-b, and Ti-w catalysts, Ti-a has a higher intensity of characteristic peaks for the OH group. The presence of OH group and water adsorbed on the catalyst surface advantaged the formation of hydroxyl free radical $HO^{\bullet}$, limited the recombination of the electron with the hole, and enhanced the photoactivity of the catalyst.

Table 3.1. Phase composition: anatase (A), brookite (B) and rutile (R), crystal size (d_{cry}), particle size (d_{par}), specific surface area (S_{BET}), pore volume (V_{pore}), pore diameter (d_{pore}), bandgap energy (E_g), absorption wavelength (λ), and point of zero charges (PZC) of TiO_2 catalysts.

Catalyst	Phase composition, %/d_{cry}, nm			d_{par}, nm	S_{BET}, m^2/g	V_{pore}, mL/g	d_{pore}, nm	E_g, eV	λ, nm	PZC
	A	B	R							
P25	86.4/ 15.1	–	13.6/ 22.7	20–25	59.6	0.060	2.44	3.25	382	4.6
Ti-a	61.3/ 7.9	20.7/ 11.3	18.0/ 14.1	5–10	58.7	0.076	2.50	3.08	403	3.1
Ti-w	100.0	–	–	5–10	84.8	0.100	2.20	3.14	395	6.9
Ti-b	–	100.0	–	30–50	16.8	0.021	2.34	3.23	384	8.0

The bandgap energy values of the Ti-a, Ti-w, and Ti-b catalysts, determined from the Tauc graph, were 3.08, 3.14; 3.23 eV, respectively; which was smaller than P25 (3.25 eV), corresponding to the longer wavelength of the absorbed light than that of P25 (382 nm), being 403, 395, and 384 nm, respectively (Figure 3.1d). The PZC values of the catalysts Ti-a, P25, Ti-w, and Ti-b were 3.1, 4.6, 6.9, and 8.0, respectively (Figure 3.1e), increasing gradually with the pH of the synthesis medium.

TEM images (Figure 3.1g–j) indicated that the P25, Ti-a, and Ti-w catalysts consisted of spherical particles 5–10 nm in size (Ti-a and Ti-w) and 20–25 nm (P25). Meanwhile, the Ti-b catalyst made of rod-shaped particles with 30-50 nm length was agglomerated into blocks and large flat plates

(Figure 3.1j). With such a structure and phase composition of 100% brookite, Ti-b catalyst had a small specific surface area and pore volume of 16.8 m^2/g and 0.021 mL/g, respectively. In contrast, the Ti-w catalyst with 100% anatase phase composition and the smallest particle size had the highest specific surface area (84.8 m^2/g) and pore volume (0,100 mL/g). P25 and Ti-a had similar phase composition and structure, so they have approximately the same specific surface area and pore volume, ranking second among TiO_2 catalysts. The adsorption-desorption isotherm of TiO_2 catalysts belonging to type IV with hysteresis loop at relative pressure $P/P_o > 0.5$ was typical for mesoporous materials, cylindrical pores, approximately 2 nm in diameter. (Figure 3.1e). Changing the hydrothermal medium made it possible to comprehensively change the phase composition, physicochemical properties, band gap energy, and PZC of TiO_2. All of these were considered to be the cause affecting the optical activity of TiO_2 catalysts.

3.1.2. Photoactivity at different pH of CA solution

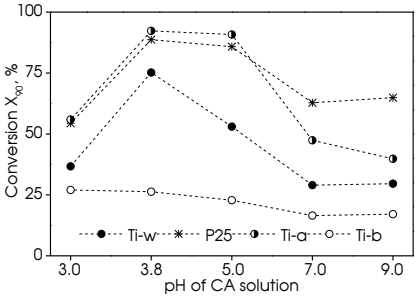

Figure 3.2. Photoactivity of TiO_2 catalysts at different pH (reaction conditions: C_{cat} = 0.25 g/L, C_{CA} = 50 mg/L, Q_{air} = 0.3 L/min, T = 25 ^oC).

The phase composition of the TiO_2 catalysts indirectly influenced the photoactivity. Ti-w catalyst in the presence of 100% anatase and the Ti-b catalyst containing the phase-pure brookite had low photoactivity. In contrast, the catalyst containing a phase mixture of Ti-a (anatase/brookite/rutile) and P25 (anatase/rutile) exhibited higher photocatalytic activity. The presence of an anatase/rutile phase mixture enhanced the catalytic activity compared to the ones in the presence of a single phase (Figure 3.2). This happens because electron transfer occurring in the mixed phases increased the charge division and prolongs the lifetime of photogenerated charges. Ti-a catalyst exhibited higher activity than in the acidic medium (pH < 5) but lowered in the high pH region compared to commercial P25. This may be related to the PZC value of the material. Thus, using the hydrothermal method and changing the medium, TiO_2

nanoparticles can be synthesized with superior properties, smaller bandgap energy, and higher photocatalytic activity than commercial P25 in the acidic medium.

3.2. Titanate-based perovskite and titanate-based pseudobrookite catalyst (MTO)

The research results show that the nanostructured rich-phase catalysts, including Al_2TiO_5 (ATO), Fe_2TiO_5 (FTO), and $CoTiO_3$ (CTO) were successfully synthesized by sol-gel method from the corresponding nitrate salts and TTIP, combined with citric acid as a complexing agent. The suitable conditions as calcination temperature and time for ATO, FTO, and CTO were 700 °C-3 h, 700 °C-2 h, and 650 °C-2 h, respectively. The physicochemical and photochemical properties of perovskite and pseudobrookite are summarized in Table 3.2 and Figure 3.3.

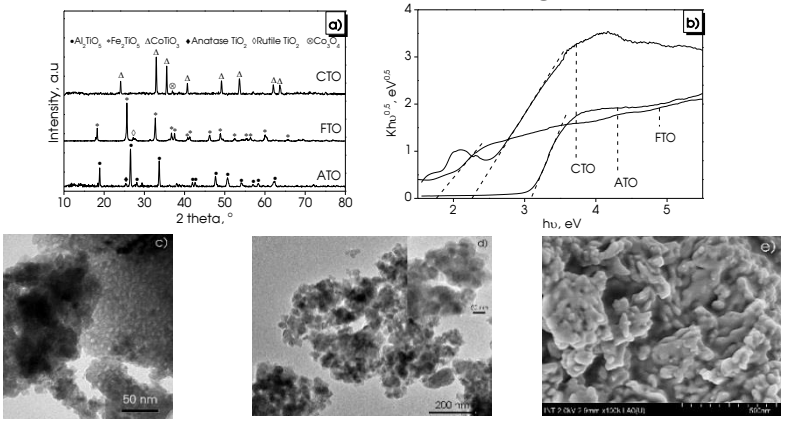

Figure 3.3. XRD pattern (a), Tauc plot (b) of the catalysts: ATO, FTO, and CTO; TEM images (c, d) of ATO and FTO catalysts; SEM image (e) of the CTO catalyst.

The XRD pattern (Figure 3.3a) demonstrated that crystalline-rich Al_2TiO_5, Fe_2TiO_5, and $CoTiO_3$ catalysts were successfully synthesized. ATO, FTO, and CTO crystal sizes were approximately the same, ranging from 31.3–36.0 nm. In addition, there were also anatase TiO_2 appeared on the ATO catalyst, rutile TiO_2 on the FTO catalyst, and rutile TiO_2 as well as Co_3O_4 on the CTO catalyst. The formation of the Fe_2TiO_5 phase on the FTO catalyst was confirmed through Raman spectroscopy. FTIR spectra indicated the presence of OH groups on the catalyst surface at the wavelength range of 3000–3750 cm^{-1} and the OH groups of water adsorbed onto the surface at

1624 cm^{-1}.

TEM and SEM images show that ATO, FTO, and CTO catalysts were composed of spherical particles with sizes of about 5–10, 20–35, and 30–60 nm, respectively, linked together into large blocks (Figure 3c–e). Therefore, perovskite and pseudobrookite had a small specific surface area and pore volume. However, 1.8–2.2 nm pore diameter would be suitable for CA degradation. The bandgap energy of the FTO catalyst (E_g = 1.74 eV) and CTO catalyst (E_g = 2.26 eV) were extremely low, absorbing the visible light of λ = 713 and 549 nm, respectively. In contrast, ATO catalyst with a high bandgap energy (E_g = 3.18 eV) absorbed UV-A light (λ = 390 nm). However, ATO had the highest specific surface area and smallest particle size among the three kinds of catalyst.

Table 3.2. Physical and chemical properties of ATO, FTO, and CTO catalysts.

Catalyst	d_{par}, nm	d_{cry}, nm	S_{BET}, m^2/g	V_{pore}, mL/g	d_{pore}, nm	E_g, eV	λ, nm	PZC
ATO	5–10	33.6	26.8	0.028	2.16	3.18	390	6.2
FTO	20–35	31.3	18.1	0.008	1.80	1.74	713	6.3
CTO	30–60	36.0	11.4	0.005	1.80	2.26	549	6.9

The citrate sol-gel method has successfully prepared perovskite and pseudobrookite with low band gap energy, suitable pore size, and neutral PZC. The results show that perovskite CTO and pseudobrookite (ATO and FTO) had suitable physicochemical and photochemical properties for photocatalysis. However, the disadvantages of ATO, FTO, and CTO were low specific surface area and small pore volume, which led to low activity in CA photodegradation. After 360 min, the highest conversion was 88.9% for ATO, 24.0% for FTO, and 19.7% for CTO. The conversion at 60 min reached 34.0, 5.0, and 4.5% compared to the Ti-w catalyst of 62.4% at reaction conditions: C_{cat} = 0.75 g/L, Q_{air} = 0.3 L/min, and pH = 3.8.

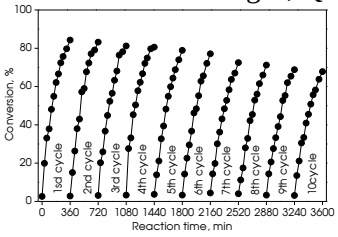

Figure 3.4. Reusability of ATO catalyst.

The ATO catalyst had the highest activity among the MTO samples due to the smallest particle size, the largest specific surface area, and the highest pore volume compared to the MTO catalysts. In addition, the ATO catalyst had good stability. After ten times being reused, the activity decreased by only 17% (Figure 3.4).

In the next section, to narrow the bandgap energy and enhance the photoactivity of TiO_2, heterostructured catalysts were fabricated by combining Ti-w with MTO catalysts: ATO-700-3, FTO-700-2, and CTO-650-2 denoted by ATO, FTO, and CTO, respectively.

3.3. Titanate-based perovskite/TiO_2 and titanate-based pseudobrookite/TiO_2 catalyst (MTO/Ti)

The presence of MTO significantly changed the photoactivity of the catalysts (Figure 3.5). The most suitable MTO content to form ATO/Ti, FTO/Ti, and CTO/Ti heterostructured catalysts are 33%ATO, 10%FTO, and 5%CTO, respectively. After 60 minutes of reaction, the CA conversion on 33ATO/Ti, 10FTO/Ti, and 5CTO/Ti catalysts are 70.1, 76.4, and 72.5%, respectively. Meanwhile, this rate of the Ti-w catalyst is lower, which is 67.1%, and those of the corresponding MTO catalysts are much lower, which include ATO (34.0%), FTO (5.0%), and CTO (4.5%).

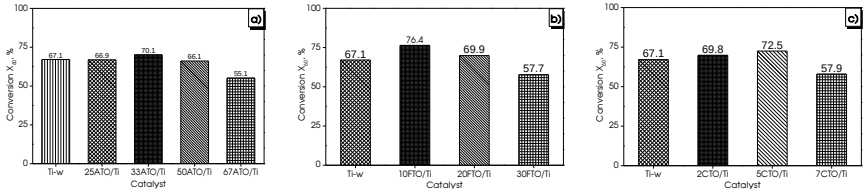

Figure 3.5. The CA conversion after a 60-minute reaction of catalysts: ATO/Ti(a), FTO/Ti(b), and CTO/Ti(c).

Table 3.3. Physicochemical and photochemical properties of MTO/Ti heterostructure catalysts.

Catalyst	d_{XRD}, nm		S_{BET}, m^2/g	V_{pore}, mL/g	d_{pore}, nm	E_g, eV	λ, nm	X_{90}, %
	TiO_2	MTO						
Ti-w	7.1	–	84.8	0.100	2.44	3.14	395	75.2
ATO	–	33.6	26.8	0.028	2.16	3.18	390	44.2
25ATO/Ti	7.2	33.0	135.1	0.081	1.78	3.07	404	75.6
33ATO/Ti	7.0	33.7	209.3	0.268	2.40	3.06	405	77.5
50ATO/Ti	7.9	32.6	103.5	0.064	1.84	3.04	408	75.1
FTO	–	30.9	18.1	0.022	2.28	1.74	713	8.5
10FTO/Ti	6.7	29.9	163.2	0.178	2.20	3.05	407	89.0
20FTO/Ti	7.9	30.9	86.3	0.053	2.00	3.05	407	79.4
CTO	–	39.9	11.4	0.005	1.80	2.26	549	4.6
2CTO/Ti	6.9	29.9	–	–	–	–	–	79.7
5CTO/Ti	7.9	30.9	130.5	0.171	2.44	3.14	395	80.9
7CTO/Ti	8.5	31.5	120.7	0.078	2.10	3.10	400	66.5

The physicochemical properties of heterostructure catalysts with different MTO contents are summarized in Table 3.3. The attendance of MTO increased the surface area, porosity, and light absorption, limiting the band gap energy and the recombination of the electron-hole pairs, which works better than Ti-w. This is considered the main reason for the improved activity of MTO/Ti catalysts compared to MTO and Ti-w catalysts. Adjusting the MTO content in each MTO/Ti catalyst group does not affect much the crystal size of MTO and TiO_2, nor the photoactivity of the catalyst. In each catalyst group, 33ATO/Ti, 10FTO/Ti, and 5CTO/Ti have the highest value of the specific surface area and pore volume. However, excess MTO decreased the specific surface area, increased electron-hole recombination, and obscured the active sites on the surface of the TiO_2 phase, reducing the catalytic activity. Figure 3.6 shows the basic properties of the best heterostructure catalysts: 33ATO/Ti, 10FTO/Ti, and 5CTO/Ti.

XRD pattern and Raman spectra of the catalysts confirmed the formation of anatase TiO_2 and Al_2TiO_5 in ATO/Ti, phase Fe_2TiO_5 in FTO/Ti and $CoTiO_3$ in CTO/Ti (Figure 3.6a). The presence of OH groups on the catalyst surface and the OH groups of water adsorbed on the surface was confirmed by FTIR spectra. Figure 3.6c shows the adsorption-desorption isotherms of type IV catalysts with hysteresis rings characteristic of capillary condensation of medium capillary materials. The adsorption-desorption isotherms of the catalysts: ATO/Ti, FTO/Ti, and CTO/Ti all have a combination of the adsorption-desorption isotherms of Ti-w and MTO. The combination of the two materials expanded the hysteresis zone pressure from > 0.8 to > 0.5, the adsorption-desorption isotherm increased, and the gap between the two adsorption-desorption arms widened than MTO and Ti-w, resulting in increased specific surface area. Among the MTO/Ti catalysts, the 33ATO/Ti catalyst has the widest adsorption-desorption branch spacing and the highest rising isotherm, thus having the highest specific surface area. The surface area of 10FTO/Ti is second and 5CTO/Ti is third. The specific surface area on the catalysts increases in the order: MTO < Ti-w < 5CTO/Ti < 10FTO/Ti < 33ATO/Ti (Table 3.3). The addition of MTO tends to decrease the bandgap energy of the heterostructure catalyst. The 33ATO/Ti and 10FTO/Ti catalysts have bandgap energies reduced to 3.05 and 3.06 eV. In comparison, adding a small amount of CTO (5%) has little effect on the band

gap energy of the heterostructure catalyst.

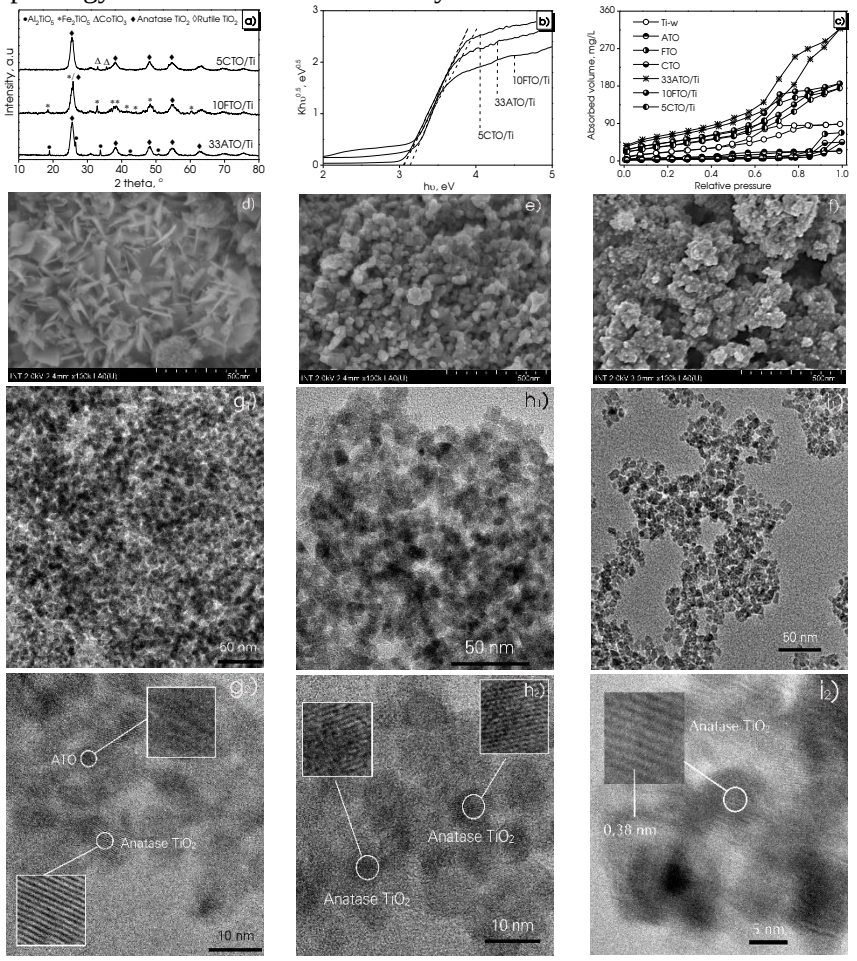

Figure 3.6. XRD pattern (a), Tauc plot (b), adsorption-desorption isotherm (c), SEM images (d–f), and HR-TEM images (g–i) of the 33ATO/Ti, 10FTO/Ti, and 5CTO/Ti catalysts.

SEM images (Figure 3.6d–f) and TEM images (Figure 3.6g–i) show that the ATO/Ti catalyst has two types of particles with different morphology. The square-shaped particles are about 100 nm and about 1–2 nm thick, which were arranged to form empty cages. Meanwhile, the spherical particles, with a size of 3–5 nm, are aggregated in pistil-shaped blocks with a 50–150 nm diameter and dispersed inside the empty cages.

Meanwhile, the FTO/Ti and CTO/Ti catalysts are spherical, with a 20–35 nm particle size. The arrangement of the spherical particles creates slits about 0.34–0.38 nm thick that make up the secondary surface. In particular, when combined with TiO_2, the 50–70 nm × 100 nm rod-shaped CTO particles that adhered to a large block in the $CoTiO_3$ changed to a separate sphere with a size of a few nm. Therefore, compared with the corresponding MTO, the specific surface area of the mixed MTO/Ti catalyst is significantly improved (Table 3.3).

In general, the MTO/Ti heterostructure catalysts have similar physicochemical properties: the crystal size of anatase TiO_2 is approximately 7 nm, the MTO is about 30 nm, and the pore diameter is about 2 nm. The isoelectric point of the 33ATO/Ti and 10FTO/Ti catalysts is 6.4 and 5CTO/Ti is 6.6. Therefore, the CA photodegradation activity of the MTO/Ti catalysts is not much different (Figure 3.5). In heterostructure catalysts, FTO/Ti has the smallest bandgap energy and widens light absorption to the visible region, so it has the highest activity. The 5CTO/Ti catalyst has high bandgap energy and a smaller specific surface area than the 33ATO/Ti catalyst. However, it has a higher activity because of the strong interaction between $CoTiO_3$ and TiO_2 to create a cross-faceted surface, increasing electron mobility and slowing down photogenerated electron-hole recombination.

The reusability of photocatalysts plays an essential role in practical applications. The reusability of the Ti-w, 33ATO/Ti, 10FTO/Ti, and 5CTO/Ti catalysts was investigated under optimal reaction conditions for each catalyst. Figure 3.7 shows the CA conversion of the catalysts. An experiment was carried out with six reuse cycles; each reaction cycle time was 90 min. The obtained results showed that the 33ATO/Ti, 10FTO/Ti, and 5CTO/Ti catalysts have better durability than the Ti-w catalyst. After six reuse cycles, the X_{90} conversion on the 33ATO/Ti, 10FTO/Ti, and 5CTO/Ti catalysts decreased compared to the X_{90} initial conversion of 30.1, 33.8, and 38.0%, respectively, meanwhile on the Ti-w catalyst has decreased by 48.0%. The decrease in CA conversion after cycles of use may be due to the amount of catalyst lost during recovery, separating the catalyst from the solution to proceed with the next batch of reactions. In heterostructure catalysts, when increasing the MTO content, the activity reduction rapidly decreases after the reuse times. The Ti-w catalyst had the highest reduction, followed by 5CTO/Ti, 10FTO/Ti, and the least on the 33ATO/Ti sample. It

was because the MTO materials have a higher density than Ti-w, leading to the result that the 5CTO/Ti, 10FTO/Ti, and 33ATO/Ti could be recovered more quickly than the Ti-w catalyst.

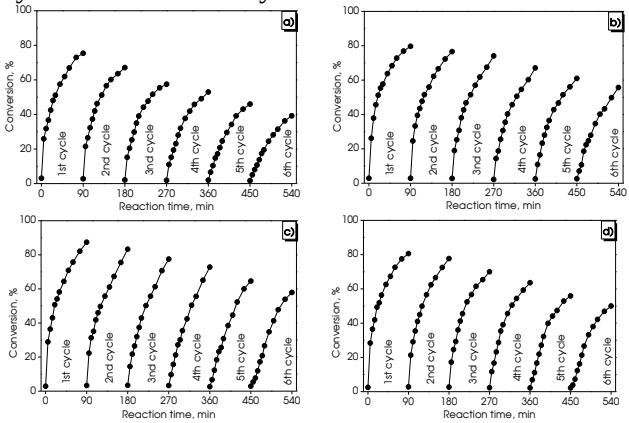

Hình 3.7. Reusability of catalysts: Ti-w (a), 33ATO/Ti (b), 10FTO/Ti (c), and 5CTO/Ti (d).

3.4. Kinetics of CA photodegradation

3.4.1. Effect of the reacting components

The influence of reaction conditions on the photocatalytic degradation rate of CA is summarized in Figure 3.8. Figure 3.8a indicates that the reaction rate increases non-linearly as the dissolved O_2 concentration increases. Therefore, O_2 concentration is involved in both the numerator and denominator of the kinetic equation. Besides, the reaction still occurred without air, although the CA conversion was relatively low. The obtained results show that several oxidizing species participated in photodegradation besides dissolved O_2.

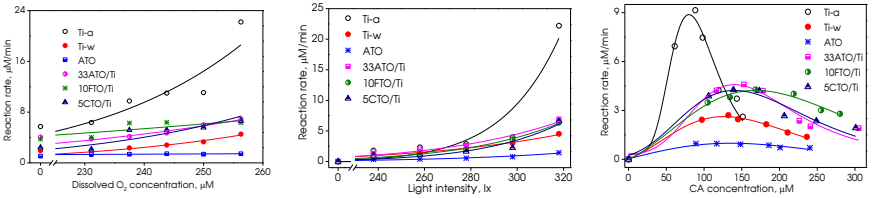

Figure 3.8. Dissolved O_2 concentration-dependence (a), light intensity-dependence (b), and CA concentration-dependence (c) of reaction rate on catalysts at X_{CA} = 30%.

The light intensity-dependence of reaction rate illustrated in Figure 3.8b showed that CA degradation does not occur without irradiation. The reaction rate increased as the light intensity increased. The reason is that

there are photons to excite to produce electron-hole pairs. The reaction rate is linearly proportional to the light intensity. The obtained results show that the light intensity I is present on the numerator of the kinetic equation in the form of I^{β}.

The CA concentration-dependence of reaction rate (Figure 3.8c) followed a parabola. The reaction rate increased with the CA concentration in the low CA concentration zone but decreased as the CA concentration increased in the zone of high CA concentration. The results demonstrate that CA concentration participated in both the numerator and denominator of the kinetic equation, and the order in the denominator was higher than in the numerator.

3.4.2. Effect of concentration of oxidizing species

In order to quantify the relative concentrations of oxidizing species on the Ti-w, Ti-a, ATO, 33ATO/Ti, 10FTO/Ti, and 5CTO/Ti catalysts, the different scavengers varying concentrations were added to the reaction solution. Salicylic acid (SA), benzoquinone (BQ), and potassium iodide (KI) were used to capture hydroxyl radicals $HO^{\bullet}$, superoxide radicals $OO^{\bullet-}$, and holes h^{+}, respectively. The influence of the density of oxidizing species on the photodegradation reaction can be assessed from the value of CA concentration at different reaction times.

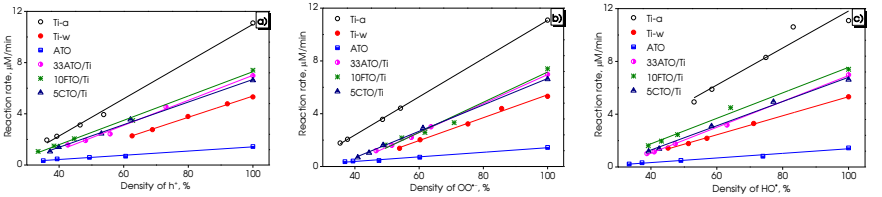

Figure 3.9. The density of oxidizing species-dependence of reaction rate on the catalysts at X_{CA} = 30%: $HO^{\bullet}$ (a), $OO^{\bullet-}$ (b), and h^{+} (c).

Table 3.4. The equation for the density of oxidizing species-dependence of reaction rate on catalysts at X_{CA} = 30%.

Catalyst	Hydroxyl radicals $HO^{\bullet}$	Superoxide radicals $OO^{\bullet-}$	holes h^{+}
Ti-a	$0.140 \times D - 2.201$	$0.145 \times D - 3.405$	$0.145 \times D - 3.549$
Ti-w	$0.072 \times D - 1.882$	$0.087 \times D - 3.233$	$0.083 \times D - 2.893$
ATO	$0.017 \times D - 0.364$	$0.017 \times D - 0.308$	$0.016 \times D - 0.225$
33ATO/Ti	$0.098 \times D - 2.870$	$0.110 \times D - 4.014$	$0.098 \times D - 2.757$
10FTO/Ti	$0.097 \times D - 2.104$	$0.114 \times D - 4.283$	$0.095 \times D - 2.208$
5CTO/Ti	$0.092 \times D - 2.385$	$0.100 \times D - 3.320$	$0.088 \times D - 2.141$

The reaction rate dependence on the density of oxidizing agents is linear: $r = a \times D + b$ (Figure 3.9). On the catalysts, the coefficient a of the $HO^{\bullet}$, $OO^{\bullet-}$, and h^{+} were approximately the same, indicating that the oxidizing agents have the same role in the CA degradation process (Table 3.4). The coefficient a on the catalysts decreased in the order: Ti-a > MTO/Ti > Ti-w > ATO, which coincided with their activity order. Therefore, it can be seen that the influence of oxidizing agents is represented by coefficient a, an index that determines the photocatalytic activity of the samples. The coefficient (a) of the Ti-a catalyst was about 1.5 times, twice, and ten times that of the MTO/Ti, Ti-w, and ATO catalysts, respectively. Ti-a catalyst has the highest coefficient (a) value of all three oxidizing species, so it has the best photoactivity. In contrast, the ATO catalyst has the lowest coefficient (a), leading to the lowest photocatalytic activity. For monocomponent catalysts (ATO, Ti-w, and Ti-a), the coefficient (a) and the CA conversion increased in the following order: ATO < Ti-w < Ti-a. When combining MTO with Ti-w to form a heterostructured catalyst MTO/Ti, the photocatalytic activity significantly increased compared to Ti-w and MTO. Simultaneously, the coefficient value of all three types of oxidizing species also increased. The results indicated that the heterostructure MTO/Ti catalysts generated more oxidizing species than Ti-w and MTO. On the catalysts ATO/Ti, FTO/Ti, and CTO/Ti, the coefficient value of hydroxyl radicals $HO^{\bullet}$ increased by 28–36%, superoxide radicals $OO^{\bullet-}$ increased by 15–26%, and holes h^{+} increased by 6–18% in comparison to the Ti-w catalyst. Therefore, the introduction of MTO produced the most hydroxyl radicals $HO^{\bullet}$, followed by superoxide radicals $OO^{\bullet-}$, and the minor holes h^{+}.

3.4.3. Intermediate compounds

The by-products formed in the reaction were analyzed from the solution of 50% CA-conversion by the HNMR method and are listed in Table 3.4. The results of the HNMR analysis showed that, in the reaction solution, there were 15 by-products and unconverted CA. The by-products are formed mainly by the different creaking of the branched chain of the CA molecule. However, based on the signal intensity of the by-products compared to the

remaining CA signal, it was found that they were present at very low concentrations in trace form. Therefore, the products of CA degradation were considered to have only the formation of CO_2 and H_2O. The concentrations of the by-products were extremely low so that they could be ignored.

3.4.4. The kinetic equation for the CA degradation

From the results of the kinetic study, the following characteristics of the kinetics for CA degradation can be given:

(i) The reaction was inhibited by at least one of the reaction products, and the kinetic equation can be fractional rather than exponential.

(ii) CA concentration is present on the numerator and denominator of the kinetic equation. The order of CA in the denominator must be greater than in the numerator.

(iii) The reaction rate was proportional to the light intensity I.

(iv Oxidizing species ($HO^{\bullet}$, $OO^{\bullet-}$, and h^+) participated in photooxidation. The reaction rate was proportional to the density of hydroxyl radicals $HO^{\bullet}$, superoxide radicals $OO^{\bullet-}$, and holes h^+. Therefore, the sum of the quantities $k_{HO^{\bullet}} C_{HO^{\bullet}} + k_{OO^{\bullet-}} C_{OO^{\bullet-}} + k_{h^+} C_{h^+}$ will appear in the numerator of the kinematic equation.

(v) The by-products presented in the solution in the trace were ignored. The obtained products in the CA degradation were considered to include only CO_2 and H_2O.

From the experimental results, the kinetic equation for CA photodegradation under UV-A light was proposed as the following

$$r = \frac{k \times \left(k_{HO^{\bullet}} C_{HO^{\bullet}} + k_{OO^{\bullet-}} C_{OO^{\bullet-}} + k_{h^+} C_{h^+} \right) \times C_{CA}^{n_1} \times C_{O_2}^{n_2} \times I^{\beta}}{\left(1 + k_1 C_{CA}^{m_1} + k_2 C_{CA}^{m_2} + k_3 C_{O_2}^{m_3} + k_4 C_{CO_2}^{m_4} + k_5 C_{Int}^{m_5} \right)^{2\alpha}} \quad (3.1)$$

Calculation of kinetic data according to equation (3.1) shows the best agreement between experimental data and calculation when the kinetic equation has the form (3.2):

$$r = \frac{k \times \left(k_{HO^{\bullet}} C_{HO^{\bullet}} + k_{OO^{\bullet-}} C_{OO^{\bullet-}} + k_{h^+} C_{h^+} \right) \times C_{CA}^{0.5} \times C_{O_2} \times I^{\beta}}{\left(1 + k_1 C_{CA}^{0.5} + k_2 C_{CA} + k_3 C_{O_2} + k_4 C_{CO_2} \right)} \quad (3.2)$$

The value of reaction order and kinetic coefficients on different catalysts were illustrated in Table 3.5.

Table 3.5. Reaction order values and kinetic coefficients of catalysts.

Parameters	Catalyst					
	Ti-a	Ti-w	ATO	33ATO/Ti	10FTO/Ti	5CTO/Ti
k, $\mu M^{-0.5}\times lx^{-\beta}\times min^{-1}\times mg^{-1}$	$1{,}83\times10^{-7}$	$1{,}94\times10^{-7}$	$2{,}22\times10^{-5}$	$1{,}98\times10^{-6}$	$3{,}91\times10^{-7}$	$3{,}91\times10^{-7}$
$k_{HO\bullet}$, μM^{-1}	$9{,}06\times10^{-2}$	$4{,}83\times10^{-2}$	$7{,}58\times10^{-3}$	$6{,}83\times10^{-2}$	$6{,}80\times10^{-2}$	$6{,}50\times10^{-2}$
$k_{OO\bullet-}$, μM^{-1}	$1{,}58\times10^{-1}$	$5{,}21\times10^{-2}$	$7{,}56\times10^{-3}$	$7{,}90\times10^{-2}$	$8{,}10\times10^{-2}$	$7{,}10\times10^{-2}$
k_{h^+}, μM^{-1}	$1{,}56\times10^{-1}$	$5{,}10\times10^{-2}$	$7{,}45\times10^{-3}$	$7{,}18\times10^{-2}$	$6{,}14\times10^{-2}$	$5{,}44\times10^{-2}$
n_1	0,5	0,5	0,5	0,5	0,5	0,5
n_2	1,0	1,0	1,0	1,0	1,0	1,0
β	2,53	2,54	1,86	2,07	2,57	2,49
k_1, $\mu M^{-0.5}$	1,263	0,006	0,074	0,046	0,045	0,041
k_2, μM^{-1}	0,033	0,003	0,005	0,003	0,003	0,009
k_3, μM^{-1}	0,0125	0,126	0,570	0,073	0,162	0,002
k_4, μM^{-1}	3,540	2,170	3,503	2,993	8,938	4,686
k_5, μM^{-m5}	0	0	0	0	0	0
m_1	0,5	0,5	0,5	0,5	0,5	0,5
m_2	1,0	1,0	1,0	1,0	1,0	1,0
m_3	1,0	1,0	1,0	1,0	1,0	1,0
m_4	1,0	1,0	1,0	1,0	1,0	1,0
α	0,5	0,5	0,5	0,5	0,5	0,5
Experimental error, %	25,8	20,3	12,1	21,0	22,9	22,6

The results show that the kinetics of CA degradation on different catalysts: TiO_2, MTO, and MTO/Ti, followed the Langmuir-Hinshelwood model. The reactants participate in the reaction (O_2 and CA) in the adsorbed state. CA existed in the form of dissociative adsorption (m_1 = 0.5) and associative (m_2 = 1.0), in which the dissociated CA form predominated with coefficient $k_1 >> k_2$. Therefore, the adsorbed CA dissociated into the reaction and appeared in the numerator (n_1 = 0.5). The order of CA in the denominator was higher than in the numerator (1.5 compared to 0.5), consistent with the extreme dependence of the reaction rate on the CA concentration. Among the catalysts, Ti-a had the highest value of k_1 and was much higher than that of other catalysts 3.5–10.0 times, so the extreme peak was the highest.

Oxygen participates in the reaction in the molecular adsorption state (m_3 = 1.0). The combination of MTO with Ti-w changed the O_2 adsorption as shown by the value of k_3, affecting the durability of the MTO/Ti catalysts: compared with Ti-w, two catalysts (33ATO/Ti and 5CTO/Ti) had a lower k_3. In comparison, the 10FTO/Ti catalyst had a higher k_3. The decrease in the k_3 value led to a decrease in O_2 inhibition. However, on FTO/Ti catalysts, the

high k_3 value was associated with the highest $k_{OO^{\bullet-}}$ constant value among the MTO/Ti heterostructure catalysts, so the 10FTO/Ti catalyst had the highest activity. In addition, the 10FTO/Ti catalyst also had high light efficiency (high β), which was also a factor creating the high activity of the catalysts.

The density of oxidizing agents: hydroxyl radicals $OH^{\bullet}$, superoxide radicals $OO^{\bullet-}$, and holes h^+ were one of the factors that directly determined the activity of the catalysts. The order of a, $k_{HO^{\bullet}}$, $k_{OO^{\bullet-}}$, and k_{h+} values was roughly the same as that of the catalyst activity. The presence of MTO increased the values of coefficients a, $k_{HO^{\bullet}}$, $k_{OO^{\bullet-}}$, and k_{h+}, so the photoactivity of the catalyst improved. Besides, the correctness of the kinetic model was shown through the complete overlap between the ratio $k_{HO^{\bullet}} : k_{OO^{\bullet-}} : k_{h+}$ with $a_{HO^{\bullet}} : a_{OO^{\bullet-}} : a_{h+}$. Among the catalysts, $k_{OO^{\bullet-}}$ and $a_{OO^{\bullet-}}$ have the highest values, indicating that the $OO^{\bullet-}$ the agent has the most influence on the photoactivity of the catalysts. Besides, the reaction rate constant k and the light efficiency β are also considered determining factors for the photoactivity of the catalysts. The β-order values on the catalysts are all greater than 1, indicating that electron-hole pairs are consumed in chemical reactions faster than in recombination. The ATO catalyst has the lowest β value and thus has the lowest activity, despite the highest apparent rate constant k. The influence of β value is clearly shown on heterostructure catalysts and determines the activity of heterostructured catalysts: 10FTO/Ti > 5CTO/Ti > 33ATO/Ti. It can be seen that the density of oxidizing agents ($OH^{\bullet}$, $OO^{\bullet-}$, and h^+) and the efficiency of light use β are decisive factors for the photoactivity of the catalysts. The order of reaction rate constant k does not coincide with the order of activity, indicating that the kinetic coefficient k value has a complex relationship with the properties of the catalyst and does not represent the catalytic activity.

CO_2 appearing in the denominator of the kinetic equation indicates that CO_2 inhibited the reaction. The presence of MTO on the heterostructure catalyst increased the CO_2 adsorption coefficient, which led to an increase in

the inhibition of the CO_2 reaction and, at the same time, increased the oxidation of the deposited coke. This was considered to cause the increased stability of heterostructure catalysts. The combination of MTO with Ti-w enhanced the reaction rate and CO_2 adsorption, so the catalytic activity enlarged moderately, and the stability of the catalyst was encouraged. On the catalysts, the coefficient k_5 values were zero, indicating that the by-products with very low content were unaffected by the reaction rate. The obtained kinetic equations also showed that the reactants were adsorbed on the same type of active site. The exponent value $\alpha = 0.5$ indicates that the reaction occurred at the average cover surface.

CONCLUSIONS AND RECOMMENDATIONS

Conclusions

Based on the obtained results of the thesis "Synthesizing titanate-based catalyst for cinnamic acid photodegradation in water", the following conclusions are proposed:

1) The TiO_2 catalysts were successfully synthesized by the hydrothermal method. The main characteristics, such as phase composition, band gap, points of zero charges, physical and chemical properties, as well as the activity of TiO_2, could be controlled by using different hydrothermal solvents. Due to the smallest band gap energy, Ti-a achieves the highest activity among obtained TiO_2 samples and is higher than the commercial TiO_2 catalyst-Degusa P25. Meanwhile, the advantage of the Ti-w sample is using an environmentally friendly solvent in the materials synthesis and the large specific surface area of the product. The photoactivity of the TiO_2 catalysts decreased in the following order: Ti-a > P25 > Ti-w > Ti-b.

2) The sol-gel method successfully synthesized Al_2TiO_5-, Fe_2TiO_5-, and $CoTiO_3$-rich catalysts with low bandgap energy at relatively low calcination temperature. However, due to the low specific surface area, the photocatalytic activity of the synthesized catalysts was low with a conversion after 90 min of 4.6, 8.5, and 44.2%, respectively.

3) Using an aqueous medium, successfully synthesized heterostructured catalysts MTO/Ti via the sol-gel-based hydrothermal method. The composition of the best-heterostructured catalysts was determined (33%ATO/Ti, 10%FTO/Ti, and 5%CTO/Ti). This catalyst group is characterized by a high specific surface area, low bandgap energy, and strong interaction between MTO and TiO_2, which increases electron mobility and slows down electron-hole recombination. The result is increasing photocatalytic activity and improving recovery and reuse. The 90-minute conversion of CA reached 77.5, 89.0, and 80.9%, respectively, compared to 72.5% of Ti-w. In addition, heterostructured catalysts were easier to recover than the Ti-w catalyst.

4) The kinetics of CA photodegradation under UV-A light on six typical catalysts: Ti-a, Ti-w, ATO, 33ATO/Ti, 10FTO/Ti, and 5CTO/Ti were comprehensively studied and proposed. In detail, the influence of dissolved O_2, CA concentrations, light intensity, and the role of oxidizing species (h^+, $HO^{\bullet}$, and $OO^{\bullet -}$) was evaluated. Based on the various research results, the kinetic equation was proposed. The results show that the CA photodegradation under UV-A light on the catalysts follows the Langmuir-Hinshelwood model, and the following general kinetic equation was found to describe the reaction:

$$r = \frac{k \times \left(k_{HO^{\bullet}} C_{HO^{\bullet}} + k_{OO^{\bullet -}} C_{OO^{\bullet -}} + k_{h^+} C_{h^+} \right) \times C_{CA}^{0.5} \times C_{O_2} \times I^{\beta}}{\left(1 + k_1 C_{CA}^{0.5} + k_2 C_{CA} + k_3 C_{O_2} + k_4 C_{CO_2} \right)}$$

The results show that the MTO/Ti heterostructure material is a potential catalyst for treating contaminated water with phenolic compounds. The obtained catalysts and reaction kinetics can be extended and applied to remove other persistent organic compounds in polluted water.

Recommendations

The doctoral thesis “Synthesizing titanate-based catalyst for cinnamic acid photodegradation in water” makes the following recommendations:

1) Studying to propose low-cost synthesis methods in large-scale production for TiO_2 catalysts with low bandgap energy and high activity

activated under sunlight.

2) To study synthesizing perovskite and pseudobrookite catalysts using the hydrothermal method to improve specific surface area.

3) Improving the photoactivity of the mixed MTO/Ti catalyst by diversifying the MTO materials and modifying the MTO structure by partially replacing the A and B metals with other metals.

4) Comprehensive study of kinetics and mechanisms of the photodegradation of persistent organics in water by numerous methods.

NEW CONTRIBUTIONS OF THE THESIS

1) Provide a photocatalytic hydrothermal synthesis method of outstanding advantages: control of phase composition, physicochemical characteristics and surface charge, and TiO_2 catalyst activity prepared by the hydrothermal method through synthetic medium pH; low-temperature sol-gel method for fabrication of pseudobrookite (Al_2TiO_5 and Fe_2TiO_5) and perovskite ($CoTiO_3$).

2) Finding new potential photocatalysts for treating organic pollutants in water such as Ti-a, pseudobrookite Al_2TiO_5, and heterostructure catalysts MTO/Ti (33ATO/Ti, 10FTO/Ti, and 5CTO/Ti). The photocatalysts have better photodegradation activity than the commercial P25 Degussa catalyst.

3) Comprehensively researched and proposed the kinetics of the photocatalytic degradation of cinnamic acid at the actual environmental conditions of the reaction and the natural pH of CA. Quantify the influence of oxidizing agents and identify intermediate compounds. Based on different results, the kinetic equation according to the Langmuir-Hinshelwood mechanism is proposed. The feature of this kinetic model is the description of the reaction under the actual conditions of the reaction. The results improve understanding of a new group of hetero-catalytic reactions - the photocatalytic.

LIST OF PUBLISHED ARTICLES OF THE THESIS

1. Nguyen Dien Trung, Ha Cam Anh, Nguyen Tri, Phan Thi Hong Phuong and Hoang Tien Cuong, *A low temperature fabrication and photoactivity of Al_2TiO_5 in cinnamic acid degradation*, Materials Transactions, 2019, 60(9), 2022-2027. (Q2, ISSN: 1345-9678, IF: 1.377).

2. Nguyen Dien Trung, Ha Cam Anh and Nguyen Tri, *Controlling phase composition, properties and activity of TiO_2 nano-photocatalyst synthesized by hydrothermal technique in the degradation of cinnamic acid solution*, Journal of Nanoscience and Nanotechnology, 2020, 20(9), 5418-5425. (Q3, ISSN: 1533-4880, IF: 1.354).

3. Nguyen Dien Trung, Ha Cam Anh, Nguyen Tri and Luu Cam Loc, *Fabrication of TiO_2/Al_2TiO_5 nanocomposite photocatalysts*, International Journal of Nanotechnology, 2020, 17(7/8/9/10), 607-622. (Q3, ISSN: 1475-7435, IF: 0.367).

4. Nguyen Dien Trung, Nguyen Tri, Phan Hong Phuong and Ha Cam Anh, *Synthesis of highly active heterostructured Al_2TiO_5/TiO_2 photocatalyst in a neutral medium*, Journal of Nanomaterials, 2020, Article ID 6684791. (Q2, ISSN: 1687-4110, IF: 3.791).

5. Nguyen Phung Anh, Nguyen Tri, Nguyen Dien Trung, Ha Cam Anh, Hoang Tien Cuong, Nguyen Thi Thuy Van, Luu Cam Loc, *Environmentally friendly fabrication of Fe_2TiO_5-TiO_2 nanocomposite for enhanced photodegradation of cinnamic acid solution*, Advances in Natural Sciences: Nanoscience and Nanotechnology, 2022, 12(4), 045015. (Q2, ISSN: 2043-6262, IF: 2.379).

6. Ha Cam Anh, Nguyen Dien Trung, Nguyen Tri, *Green fabrication of heterostructured $CoTiO_3/TiO_2$ nanocatalyst for efficient photocatalytic degradation of cinnamic acid*, ACS Omega, 2022, 7(44), 40163-40175. (Q1, ISSN: 2470-1343, IF: 4.132).